Smart Structures and Systems, *Vol. 25, No. 6 (2020) 719-732*
DOI: https://doi.org/10.12989/sss.2020.25.6.719

Robust stability analysis of real-time hybrid simulation considering system uncertainty and delay compensation

Pei-Ching Chen* and Po-Chang Chen [a]

Department of Civil and Construction Engineering, National Taiwan University of Science and Technology, No.43, Sec.4, Keelung Rd., Taipei 10607, Taiwan

(*Received September 24, 2019, Revised February 13, 2020, Accepted March 5, 2020*)

Abstract. Real-time hybrid simulation (RTHS) which combines physical experiment with numerical simulation is an advanced method to investigate dynamic responses of structures subjected to earthquake excitation. The desired displacement computed from the numerical substructure is applied to the experimental substructure by a servo-hydraulic actuator in real time. However, the magnitude decay and phase delay resulted from the dynamics of the servo-hydraulic system affect the accuracy and stability of a RTHS. In this study, a robust stability analysis procedure for a general single-degree-of-freedom structure is proposed which considers the uncertainty of servo-hydraulic system dynamics. For discussion purposes, the experimental substructure is a portion of the entire structure in terms of a ratio of stiffness, mass, and damping, respectively. The dynamics of the servo-hydraulic system is represented by a multiplicative uncertainty model which is based on a nominal system and a weight function. The nominal system can be obtained by conducting system identification prior to the RTHS. A first-order weight function formulation is proposed which needs to cover the worst possible uncertainty envelope over the frequency range of interest. Then, the Nyquist plot of the perturbed system is adopted to determine the robust stability margin of the RTHS. In addition, three common delay compensation methods are applied to the RTHS loop to investigate the effect of delay compensation on the robust stability. Numerical simulation and experimental validation results indicate that the proposed procedure is able to obtain a robust stability margin in terms of mass, damping, and stiffness ratio which provides a simple and conservative approach to assess the stability of a RTHS before it is conducted.

Keywords: real-time hybrid simulation; system uncertainty; robust stability; delay compensation

1. Introduction

Real-time hybrid simulation (RTHS), combining physical testing with numerical simulation, is an efficient and cost-effective experimental method to investigate the seismic performance of structures subjected to earthquakes. Generally, a structure is separated into an experimental substructure and a numerical substructure in a RTHS. It is noted that the experimental substructure normally contains components or devices that are difficult to simulate accurately. The boundary degrees of freedom between the experimental and numerical substructures are represented by servo-hydraulic actuators with steel fixtures or a seismic shake table in the laboratory, namely, a servo-hydraulic transfer system. A step-by-step integration algorithm is required to solve the displacement response at the boundary degrees of freedom of the numerical substructure. This displacement then becomes the desired displacement to be imposed on the experimental substructure. The corresponding restoring force is measured from the experimental substructure and fed back to the step-by-step integration algorithm to compute the displacement response for the next time step until the entire RTHS is completed. However, the computation, communication, and dynamics of the servo-hydraulic system result in time lag and delay between the desired and achieved displacement responses, introducing negative damping into the hybrid simulation loop and leading potential instabilities (Horiuchi *et al.* 1999). As a result, RTHS has been recognized as a challenging and demanding experimental method for earthquake engineering studies as the numerical and experimental substructures must transfer the responses at the boundary degrees of freedom in real time.

In order to resolve the unstable issue due to time lag and delay, various compensation methods have been proposed and applied to RTHS. Horiuchi *et al.* (1999) proposed a compensation method based on linear acceleration extrapolation, which can be used to predict the actuator displacement by applying the Newmark family integration algorithms. Jung *et al.* (2007) applied the derivative feedforward compensation with the HHT α-method integration algorithm. Chen *et al.* (2009) derived a first-order discrete inverse compensator to compensate actuator delay. Chen and Tsai (2013) proposed a second-order discrete phase-lead compensator with online delay estimation through a gradient adaptive law. Chae *et al.* (2013) developed an adaptive time series compensator which updates the coefficients of the system model online. Phillips *et al.* (2014) proposed the backward-difference

*Corresponding author, Assistant Professor,
E-mail: peichingchen@mail.ntust.edu.tw
[a] Graduate Student, E-mail: m10705308@mail.ntust.edu.tw

http://www.techno-press.org/?journal=sss&subpage=7
ISSN: 1738-1584 (Print), 1738-1991 (Online)

method to discretize a feedforward controller in RTHS. Hayati and Song (2017) proposed a discrete feedforward compensator using finite impulse response filter formulation. Although these aforementioned methods are slightly different with respect to the order and formulation, they all aim at compensating the actuator time delay and reducing the corresponding effect on the stability of RTHS. Experimental results have demonstrated that these compensation methods are able to achieve successful and stable RTHS.

Various stability analyses have been conducted in order to realize the stability margin of a RTHS. Horiuchi *et al.* (1999) used an energy balance approach to determine the critical time delay that causes the instability of a single-degree-of-freedom (SDOF) structure in RTHS. The analytical results indicate that the time delay of actuator can be treated as an equivalent negative damping. When the negative damping resulted from actuator time delay is larger than the inherent damping of the SDOF structure, the entire RTHS becomes unstable. Wallace *et al.* (2005) derived a delay differential equation to obtain the critical time delay of a SDOF structure in RTHS. Mercan and Ricles (2007) used the pseudodelay technique (Rekasius 1980) to solve the critical time delay considering the amplitude error and delay separately for a SDOF structure. The analytical results indicate that an overshoot error adds damping to the RTHS, whereas an undershoot error decreases damping. Gonzalez-Buelga *et al*. (2007) demonstrated the effects of delay and noise on the stability of the substructuring system in which the delay was minimized by using a polynomial forward prediction technique and the noise was mitigated using a filtering technique. Chen and Ricles (2008) investigated the effect of actuator delay and integration algorithms on the stability of RTHS through the closed-loop transfer function in discrete time domain. Chen and Tsai (2013) applied the pseudodelay technique to obtain the critical time delay for a SDOF structure considering both the amplitude error and delay simultaneously. The analytical results conclude that an overshoot amplitude error makes the structural system stiffer. As a result, the critical time delay decreases when an overshoot amplitude error occurs even though it adds a positive damping to the structural system. It is noted that the aforementioned stability analyses do not consider the effect of numerical integration on the RTHS stability. Meanwhile, the dynamics of servo-hydraulic system is not considered either. Zhu *et al*. (2015) utilized the discrete-time root-locus technique to investigate the stability of multi-degrees-of-freedom (MDOF) RTHS which considered the effects of integration time step, time delay, structural property, and delay compensation. The technique was applied to shake table testing in the laboratory. Maghareh *et al*. (2017) proposed predictive stability indicator to evaluate the sensitivity of an RTHS configuration to de-synchronization at the interface of the physical specimen and numerical model and extended it to linear MDOF systems by converting a delay differential equation to a generalized eigenvalue problem using a set of vectorization mappings. Tang *et al.* (2018) used the gain margin to determine the RTHS stability of a SDOF structure considering the combined effect of varying amplitude and phase due to the dynamics of the servo-hydraulic system. Huang *et al*. (2019) used the Lyapunov-Krasovskii stability theorem to explore the stability of RTHS considering both constant and time-varying actuator delay and suggested that the assumption of constant time delay is suitable to RTHS of linear SDOF systems as long as the stiffness ratio for physical substructure is large enough.

In this study, a robust stability analysis procedure for a SDOF structure is proposed and inspected which considers the uncertainty of servo-hydraulic system dynamics with and without delay compensation. The experimental substructure is assumed to be a ratio of the stiffness, mass, and damping, respectively. Instead of the pure delay and amplitude error model, the servo-hydraulic system is represented as a fourth-order transfer function model which is treated as the nominal model. Each parameter of the nominal model has ±10% perturbation to denote the parametric uncertainty of the system. In addition, a multiplicative uncertainty model is adopted to describe the unstructured uncertainty of the servo-hydraulic system. The Nyquist plot of the RTHS loop with the perturbed servo-hydraulic system is adopted to determine the robust stability margin of the RTHS in a graphical interpretation manner. Furthermore, three commonly used delay compensation methods are considered in the stability analyses. Accordingly, the robust stability margin of RTHS in terms of the ratio of the stiffness, mass, and damping with respect to the natural frequency of the entire SDOF structure can be obtained. For the validating stage, a large number of numerical simulations are conducted which vary the stiffness ratio, mass ratio, and damping coefficient ratio of the experimental substructure to the whole structure, respectively. Meanwhile, the allow stiffness ratio is further verified by conducting RTHS in the laboratory. Finally, the results are summarized and discussed.

2. Mathematical modeling

The mathematical modeling for robust stability analyses of RTHS is introduced in this section including the servo-hydraulic system modeling, the parametric and unstructured uncertainty modeling, and the RTHS loop modeling.

2.1 Servo-hydraulic system modeling

Generally, the dynamics of a servo-hydraulic system in RTHS is composed of a servo controller, servo valve dynamics, servo-valve flow, an actuator, and a physical specimen. The block diagram of a servo-hydraulic system is illustrated in Fig. 1 in which the parameter A is the piston area and s is a complex number in the Laplace transform. The input current that drives the servo-valve is normally generated by a proportional-integral-derivative (PID) controller; however, merely the proportional gain is used for most application in RTHS. Each component of a servo-valve has its own dynamic characteristics; for example, the torque motor dynamics, and the spool valve dynamics. Therefore, the mathematical model of a servo-valve is very complicated. Merritt (1967) derived a linearized model of each component of a servo-valve which is an eighth-order transfer function. However, this high-order model considers numerous design factors, which could affect the performance of a servo-valve significantly. Mostly, the dynamic response of the servo-valve is faster than the other components in RTHS. Therefore, a simplified first-order model of the servo-valve is representative sufficiently for a frequency bandwidth from 0 Hz to 50 Hz. The fluid in the servo-valve also has its dynamic characteristics which can be represented by linearizing the nonlinear flow equation as well as applying the continuity equation and Newton's second law. The linearized flow equation connects the control flow to the valve spool displacement and the load pressure (the pressure drop across the piston) which can be indicated in the load pressure feedback in the block diagram. Lastly, the experimental substructure attached to the servo-hydraulic actuator has structural dynamics which can be formulated as a mass-spring-damper model. Noted that there is a feedback from the structural velocity response to the hydraulic flow into the actuator which is referred as natural velocity feedback. Therefore, the dynamics of the specimen directly affects the performance of servo-hydraulic actuator through this natural velocity feedback.

The derivation detail of a servo-hydraulic system can be referred to Carrion and Spencer (2007). Consequently, the mathematical model of a servo-hydraulic system in RTHS can be expressed as a four-pole transfer function

$$G_s(s) = \frac{a_0}{s^4 + a_3 s^3 + a_2 s^2 + a_1 s + a_0} \tag{1}$$

where a_3, a_2, a_1, a_0 are the identified parameters of the servo-hydraulic system that are either directly or indirectly related to each component of servo-hydraulic system as depicted in Fig. 1.

2.2 Uncertainty modeling

It is difficult to have a mathematical model that can precisely represents a physical system in real world. Modeling error of the servo-hydraulic system affects the stability margin of RTHS. Generally speaking, the identified mathematical model of a servo-hydraulic system is called the nominal model (Eq. (1)). This nominal model can be perturbed in physical practice due to noise interference, system nonlinearities, and unmodeled dynamics (Zhou and Doyle 1998). The model uncertainties can be quantified essentially by two main approaches, namely structured uncertainty and unstructured uncertainty. An uncertainty model of the servo-hydraulic system is essential for robust stability analysis in this study.

2.2.1 Parametric uncertainty

One of the structured uncertainty modeling methods is to parametrize the coefficients of a transfer function within a predefined range which is named parametric uncertainty. As aforementioned, the servo-hydraulic system in RTHS can be presented by a fourth-order transfer function with no zeros. In practice, the coefficients of the transfer function in Eq. (1) are obtained by conducting system identification. However, the servo-hydraulic system is an inherently nonlinear system. The parameters of the linearized servo-hydraulic system model depend on the operating conditions such as the laboratory temperature, signal quality, and etc. Therefore, the parametric uncertainty could affect the stability margin of RTHS. It is straightforward to consider the effects of parametric uncertainty on RTHS stability simply by setting a range of parameters for the identified mathematical model of the servo-hydraulic system as

$$\bar{G}_s(s) = \left\{ \frac{a_0}{s^4 + a_3 s^3 + a_2 s^2 + a_1 s + a_0} \quad \begin{matrix} a_{nmin} \le a_n \le a_{nmax}; \\ n = 0,1,2,3 \end{matrix} \right\} \tag{2}$$

Each identified parameter lies in a predefined interval, which depends on the quality of the testing facilities and environment in the laboratory.

2.2.2 Unstructured uncertainty

The linearized servo-hydraulic system model is adequate in low frequency with reasonable force demand. However, it may not be appropriate in high frequency range. Therefore, unstructured uncertainty is indispensable to cover the unmodeled dynamics of a servo-hydraulic system, particularly within the high frequency range. Three types of unstructured uncertainty models are mostly adopted including additive uncertainty, multiplicative uncertainty, and coprime factor uncertainty. Each type of the unstructured uncertainty model has forward or inverse formulation, leading to a large variety of unstructured uncertainty models that are available to describe the perturbation considered in RTHS. Among them, a disk-like uncertainty model has been widely used as it is simple for general analysis methods. For this reason, the multiplicative uncertainty model is adopted which can be expressed as

$$\tilde{G}_s(s) = [1 + W(s)\Delta(s)]G_s(s) \tag{3}$$

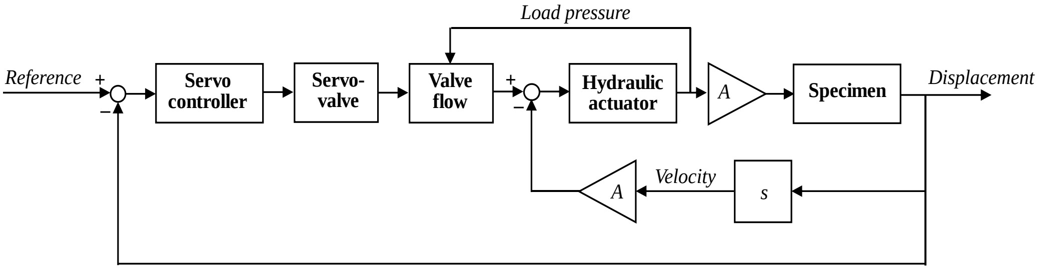

Fig. 1 Block diagram of the servo-hydraulic system for RTHS

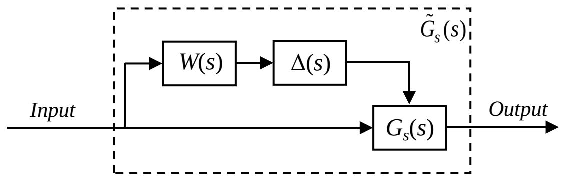

Fig. 2 Block diagram of a multiplicative uncertainty model

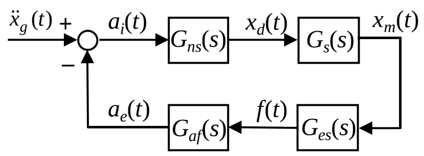

Fig. 4 Equivalent transfer functions of RTHS

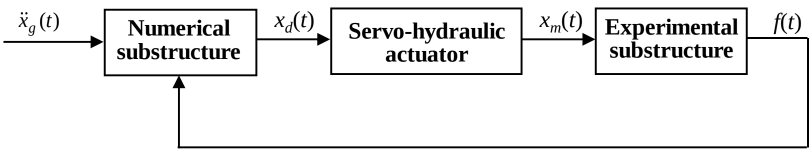

Fig. 3 General real-time hybrid simulation loop

where $\tilde{G}_s(s)$ represents the multiplicative uncertain model of the servo-hydraulic system; $W(s)$ is a stable weight function considering the distribution of the uncertainty maximum magnitude over the frequency of interest; and $\Delta(s)$ is a random stable transfer function that contains the uncertainty on the magnitude and phase perturbation. The infinity norm of $\Delta(s)$ must satisfy the following inequality

$$\|\Delta(s)\|_\infty \le 1; \quad s = j\omega \quad \forall\omega \tag{4}$$

where j represents imaginary unit and ω is the angular frequency. The block diagram of the multiplicative uncertainty is illustrated in Fig. 2. It is noted that the multiplicative uncertainty model can be characterized into input multiplicative perturbation and output multiplicative perturbation. However, the two types of multiplicative models are identical for single-input-single-output systems.

2.3 Real-time hybrid simulation loop

Real-time hybrid simulation forms a closed loop between the numerical substructure, servo-hydraulic system, and experimental substructure. Fig. 3 depicts the relationships between each primary component in RTHS. For earthquake engineering studies, the ground motion $\ddot{x}_g(t)$ is input to the numerical substructure and the corresponding displacement response at the boundary degrees of freedom needs to be imposed to the experimental substructure through the servo-hydraulic actuator in real time. However, the achieved displacement $x_m(t)$ could be different from the desired displacement $x_d(t)$ due to the dynamics of the servo-hydraulic system. The restoring force $f(t)$ is then measured and fed back to the numerical substructure and complete the RTHS closed loop.

The general RTHS loop can be further investigated from the perspective of transfer function as shown in Fig. 4. The transfer function from the input acceleration $a_i(t)$ to the desired displacement $x_d(t)$ is denoted as $G_{ns}(s)$. The desired displacement is sent to the servo-hydraulic system $G_s(s)$ and the corresponding output becomes the achieved displacement $x_m(t)$. The experimental substructure is then deformed and the corresponding force can be measured. The specimen dynamics can be represented by the transfer function $G_{es}(s)$ from the input displacement $x_m(t)$ to the restoring force $f(t)$. Finally, the restoring force can be converted into an equivalent input acceleration $a_e(t)$ for the numerical substructure by a transfer function $G_{af}(s)$. Accordingly, the corresponding closed-loop transfer function of RTHS becomes

$$x_m(t) = \frac{G_s(s)G_{ns}(s)}{1 + G_{af}(s)G_{es}(s)G_s(s)G_{ns}(s)}\ddot{x}_g(t) \tag{5}$$

Noted that Eq. (5) is abuse of notation between time domain and s domain for simplicity.

3. Robust stability analysis (stiffness term)

3.1 Nyquist stability with system uncertainty

A RTHS closed loop is robust if the internal stability for every component in the loop is provided. As mentioned before, the multiplicative uncertain model is adopted as it is simple for the stability analysis. From the robust stability theorem (Doyle *et al.* 1992), it is known that the closed-loop RTHS is robustly stable if and only if

$$\|W(s)T(s)\|_\infty < 1 \tag{6}$$

where $T(s)$ is the complementary sensitivity function of the closed-loop RTHS in Fig. 4

$$T(s) = \frac{G_{af}(s)G_{es}(s)G_s(s)G_{ns}(s)}{1 + G_{af}(s)G_{es}(s)G_s(s)G_{ns}(s)} = \frac{L(s)}{1 + L(s)} \tag{7}$$

$L(s)$ is the loop transfer function. Substituting Eq. (7) into Eq. (6), the following inequality can be obtained:

$$|W(s)L(s)| < |1 + L(s)|; \quad s = j\omega \quad \forall\omega \tag{8}$$

From the graphical interpretation, Eq. (8) indicates that the distance from (-1, 0) to the nearest point of $L(j\omega)$ should be larger than the disk-like uncertainty made by $W(j\omega)$ on the complex plane. Therefore, the Nyquist plot is helpful to providing straightforward information of the stability margin considering modeling uncertainty.

Nyquist stability criterion has been widely used to evaluate the stability of a linear time-invariant control system in which the Nyquist plot is essential for stability assessment of the control system. Details of Nyquist stability criterion and its derivation can be found in the textbooks of control theory (Doyle *et al.* 1992). Merely the most critical part adopted in this study is introduced due to the limited pages. From the Nyquist stability criterion, the stability of a closed-loop control system can be analyzed through its open-loop system transfer function by applying Cauchy's principle of argument. The Nyquist contour is formed by connecting the imaginary axis from 0 to $+j\infty$, a semicircle of infinite radius that encloses the entire right half s-plane, and the imaginary axis from $-j\infty$ to 0. Accordingly, the mapped contour in the $L(s)$-plane encircles the point (-1, 0) N times clockwise, which satisfies the following condition

$$N = Z - P \tag{9}$$

where Z is the number of unstable closed-loop poles and P is the number of unstable open-loop poles. There is no unstable pole for each RTHS component shown in Fig. 4 if the servo-hydraulic actuator is well-tuned. Therefore, the number of unstable open-loop poles is equal to zero (P = 0). As a result, the number of clockwise encirclement of the point (-1, 0) in the $L(s)$-plane should be zero (N = 0) if the closed-loop RTHS is stable (Z = 0). The loop transfer function with multiplicative uncertainty in the Nyquist plot is used to determine the stability of RTHS loop in this study. Fig. 5 illustrates the Nyquist plot with multiplicative uncertainty. Due to the fact that P = 0, it can be found that the closed-loop RTHS becomes unstable if the envelope of the disk-like uncertainty (dashed-line) encircles the point (-1, 0). In other words, the closed-loop RTHS is robustly stable if and only if the envelope of the Nyquist plot with uncertainty does not include the point (-1, 0). Noted that even though the nominal loop transfer function has fair gain margin, it does not necessarily indicate that the robust stability is guaranteed after the system is perturbed.

3.2 Robust stability of RTHS

The stability analysis of RTHS with system uncertainty was conducted following the mathematical modeling and

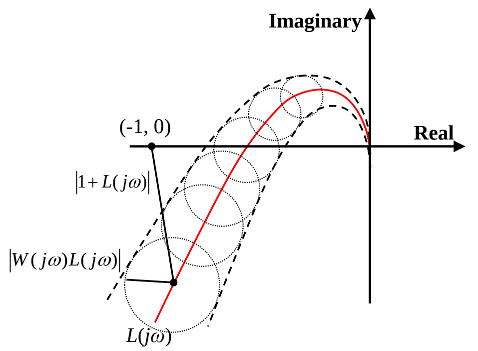

Fig. 5 Illustration of the Nyquist plot of a system with multiplicative uncertainty

stability criterion stated previously. Consider a SDOF structure in which part of the stiffness is experimentally tested. Thus, the equation of motion of the SDOF structure can be expressed as

$$\begin{aligned} &m\ddot{x}(t) + c\dot{x}(t) + (1-p_k)kx(t) \\ &= -m\ddot{x}_g(t) - p_k kx(t) \end{aligned} \tag{10}$$

where m, c, and k denote the mass, damping coefficient, and stiffness of the SDOF structure, respectively; $x(t)$, $\dot{x}(t)$, and $\ddot{x}(t)$ are the relative displacement, relative velocity, and relative acceleration of the structure, respectively; p_k is the ratio of the stiffness of the experimental substructure to the entire stiffness of the SDOF structure; and $\ddot{x}_g(t)$ is the ground acceleration. Henceforth, p_k is called the stiffness ratio in the paper for simplicity. Accordingly, the transfer function of the numerical substructure in Fig. 4 is

$$\begin{aligned} G_{ns}(s) &= \frac{-m}{ms^2 + cs + (1-p_k)k} \\ &= \frac{-1}{s^2 + 2\xi\omega_n s + (1-p_k)\omega_n^2} \end{aligned} \tag{11}$$

where ξ and ω_n represent the damping ratio and natural frequency of the structure, respectively. In the paper, the damping ratio was assumed 2% for all the robust stability analyses.

The transfer function of the servo-hydraulic system in RTHS can be obtained by conducting system identification. In the stability analysis, the rational transfer function used by Tang *et al.* (2018) was adopted which can be expressed as

$$G_s(s) = \frac{5.659 \cdot 10^9}{\begin{array}{c} s^4 + 714.5s^3 + 3.393 \cdot 10^5 s^2 \\ +6.469 \cdot 10^7 s + 5.659 \cdot 10^9 \end{array}} \tag{12}$$

Conservatively, ±10% identification error was assumed and taken as the parametric uncertainty for each parameter in Eq. (12). Noted that this range of parameters can be modified depending on the facility condition and measurement quality in the laboratory. Accordingly, the perturbed nominal transfer function of the servo-hydraulic system becomes

$$\begin{aligned} &\bar{G}_s(s) \\ &= \left\{ \frac{a_0}{s^4 + a_3 s^3 + a_2 s^2 + a_1 s + a_0} : \begin{array}{c} 643.1 \le a_3 \le 786.0 \\ 3.054 \cdot 10^5 \le a_2 \le 3.732 \cdot 10^5 \\ 5.822 \cdot 10^7 \le a_1 \le 7.116 \cdot 10^7 \\ 5.093 \cdot 10^9 \le a_0 \le 6.225 \cdot 10^9 \end{array} \right\} \end{aligned} \tag{13}$$

Fig. 6 illustrates the frequency response of the nominal servo-hydraulic system transfer function with ±10% parametric uncertainty for each parameter. It can be found that the magnitude varies significantly when the frequency is larger than 5 Hz.

The weight function used for the multiplicative uncertain model is critical to robust stability analysis as it considers the distribution of the uncertainty maximum magnitude over the frequency of interest. An appropriate weight function forms an uncertainty envelope that covers the maximum magnitude of normalized perturbed servo-hydraulic system over the considered frequency range even for the worst possible case of parametric uncertainty as indicated in Eq. (13). In other words, the distance between the weight function and the curves of normalized perturbation in the frequency domain should be as small as possible. Large distance leads to a conservative stability margin in the analysis. Generally, the weight function is obtained through trial and error process which is neither effective nor systematic. In this study, a simple but appropriate weight function is proposed to form the multiplicative uncertain model for the robust stability analysis of RTHS which can be expressed as

$$W(s) = \frac{0.85\left(s + \frac{1}{p}\right)}{s + p} \qquad (14)$$

where p represents the real part of the stable pole that is closest to the imaginary axis in the s-plane. Noted that Eq. (14) is proposed based on 10% parametric uncertainty. Accordingly, the weight function for the specific nominal transfer function (Eq. (12)) can be determined

$$W(s) = \frac{0.85s + 3.844 \cdot 10^{-3}}{s + 221.11} \qquad (15)$$

Furthermore, Eq. (3) can be normalized with respect to the nominal servo-hydraulic system as

$$\left|\frac{\tilde{G}(s)}{G(s)} \text{-}1\right| \le |W(s)|\,; \quad s = j\omega \quad \forall\omega \qquad (16)$$

which provides a graphical interpretation in frequency domain to ensure if the selected weight function is appropriate or not. Fig. 7 shows the normalized perturbed servo-hydraulic system and the proposed weight function. It is found that the proposed weight function formulation covers the normalized perturbed servo-hydraulic system over the frequency of interest. The distance between the weight function and the perturbed systems is trivial from 0.001 Hz to 100 Hz. Although the distance becomes larger when the frequency is higher than 100 Hz, it is on the conservative side for RTHS. It is demonstrated that the proposed weight function covers the uncertainty maximum magnitude fairly over the considered frequency range, providing a simple and straightforward method for selecting the weight function without trial and error. Accordingly, a proper multiplicative uncertainty model can be constructed and the corresponding robust stability can be conducted. Fig. 8 depicts the stability margin with respect to the relationship between the natural frequency of the entire structure and the stiffness ratio p_k. Merely the natural frequencies of a SDOF structure ranges from 0 Hz to 20 Hz are discussed in this study as it is common and reasonable for buildings. By using the exampled servo-hydraulic system, the entire structural stiffness can be represented by the specimen in RTHS on condition that the natural frequency of the structure is less than 0.5 Hz. In addition, the allowable stiffness ratio decreases significantly when the natural frequency of the structure increases from 0.5 Hz to 5 Hz. When the natural frequency of the structure is larger than 6 Hz, less than 10% of the structural stiffness can be taken out as the physical specimen. As a result, delay compensation becomes essential for conducting stable RTHS. Furthermore, the stability margin become a stability area when the system uncertainty is considered in RTHS as the dashed lines shown in Fig. 8. The allowable stiffness ratio does not necessarily become smaller or larger after applying the uncertainty model. However, merely the inferior allowable stiffness ratio is adopted for the following analyses from the aspect of safety in RTHS, i.e., the lower dashed curve in Fig. 8.

In order to realize whether the stability margin was conservative, a large number of numerical simulations were conducted in which the natural frequency of the structure was varied from 1 Hz to 20 Hz with an increment of 1 Hz. In addition to the allowable stiffness ratio with and without considering system uncertainty, i.e., the lower dashed curve and solid curve in Fig. 8, quartiles between the two

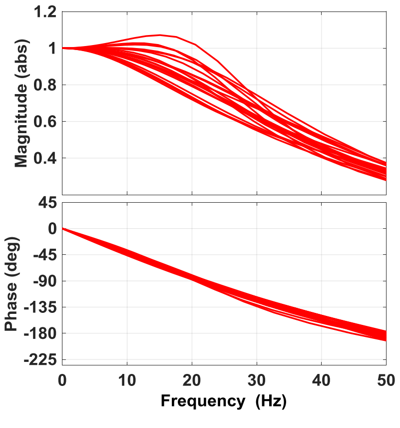

Fig. 6 Frequency response of the servo-hydraulic system with parametric uncertainty

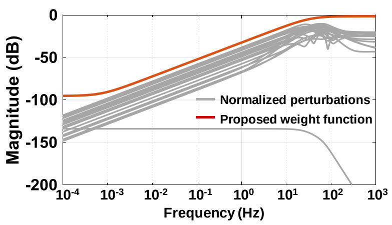

Fig. 7 Bode magnitude plot of the normalized perturbations and the proposed weight function

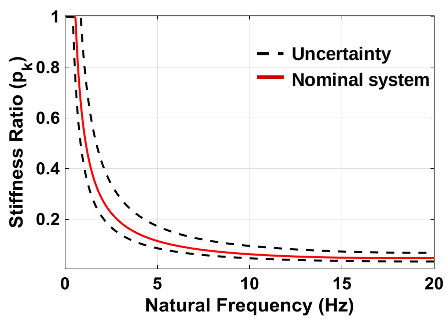

Fig. 8 Stability margin of RTHS in terms of stiffness ratio considering system uncertainty

Table 1 Unstable probability distribution of RTHS considering system uncertainty (%)

Natural frequency (Hz)	p_{ku}	$p_{ku}+\frac{1}{4}(p_{kn}-p_{ku})$	$p_{ku}+\frac{1}{2}(p_{kn}-p_{ku})$	$p_{ku}+\frac{3}{4}(p_{kn}-p_{ku})$	p_{kn}
1	0	2.58	12.37	29.07	50.09
2	0	2.34	11.63	28.87	49.69
3	0	1.41	10.79	27.98	49.22
4	0	0.42	8.74	26.29	50.12
5	0	0.07	6.95	23.78	48.68
6	0	0	4.11	22.51	50.29
7	0	0	1.39	18.96	49.66
8	0	0	0.13	14.11	49.14
9	0	0	0	9.04	48.74
10	0	0	0	5.79	47.93
11	0	0	0	3.35	46.03
12	0	0	0	3.62	42.62
13	0	0	0	5.80	44.39
14	0	0	0	9.08	44.62
15	0	0	0.05	11.95	45.27
16	0	0	0.94	15.15	47.44
17	0	0	2.61	18.60	46.78
18	0	0.07	4.38	21.00	46.74
19	0	0.12	5.71	22.62	47.12
20	0	0.40	7.72	24.45	48.21

allowable stiffness ratios were selected for simulation. The allowable stiffness ratio with and without considering system uncertainty is denoted p_{ku} and p_{kn}, respectively. Accordingly, a total number of 100 cases (20 × 5) were selected in the numerical simulation. For each case, 10,000 servo-hydraulic systems with randomly assigned parametric uncertainties bounded by ±10% of the nominal parameters were adopted. In other words, the $G(s)$ in Fig. 4 was replaced by $\bar{G}_s(s)$ (Eq. (13)) while the rest of the transfer functions remained identical in each case. The unstable probability distribution of RTHS obtained from the numerical simulations is shown in Table 1. It can be observed that there is approximate 50% probability of achieving unstable RTHS when the stiffness ratio is p_{kn} which clearly indicates that the allowable stiffness ratio for the nominal servo-hydraulic system is not robustly stable if ±10% of the parametric uncertainty is adopted. On the other hand, none of the 10,000 test cases for each natural frequency is unstable when the stiffness ratio is p_{ku}. Besides, less than 3% possibility that RTHS is unstable even when the stiffness ratio is the first quartile between p_{ku} and p_{kn}. The simulation results are slightly conservative especially when the natural frequency is between 9 Hz to 14 Hz. It can be improved by applying another weight function $W(s)$ that covers the curves of normalized perturbation with infinitesimal distance in the frequency domain; however, it could take much time by trial and error. Alternatively, the proposed weight function is easy to form and the corresponding robust stability margin is slightly conservative but adequate for RTHS stability analyses.

4. Robust stability with delay compensation (stiffness term)

4.1 Delay compensation

Three delay compensation methods were considered in the robust stability analyses in this study including the linear acceleration extrapolation (Horiuchi and Konno 2001), first-order inverse compensator (Chen *et al.* 2009), and second-order phase-lead compensator (Chen and Tsai 2013). Noted that these three compensation methods are formed in discrete time; therefore, delay steps of the servo-hydraulic system and sampling rate of the RTHS are required. Assuming that the RTHS is conducted with a sampling rate of 2,000 Hz, the nominal transfer function adopted in this study as shown in Eq. (12) has an approximate constant delay time of 11.83 msec, which is nearly equal to 24 delay time steps.

4.1.1 Linear acceleration extrapolation

Linear acceleration extrapolation (LAE) method is based on a linear acceleration assumption. In this compensation scheme, a predicted acceleration response can be obtained by extrapolating from the previous two steps of acceleration response which considers the sampling period and the actuator delay. Then, the corresponding predicted displacement can be obtained from the predicted acceleration response by applying the Newmark integration algorithm. The final delay compensator can be formed as a discrete transfer function with the coefficients shown in Table 2 in which Δt, and τ are the time step and delay time;

Table 2 Coefficients of the discrete compensator from linear acceleration extrapolation

Coefficient	Numerator	Denominator
z^4	0	$2\beta\Delta t^3$
z^3	$(4\beta + 2\gamma + 1)\Delta t^3 + (6\beta + 2\gamma + 2)\tau\Delta t^2 + (6\beta + 1)\tau^2\Delta t + 2\beta\tau^3$	$(-4\beta + 2\gamma + 1)\Delta t^3$
z^2	$(- 10\beta - 2\gamma + 1)\Delta t^3 - (18\beta + 4\gamma + 2)\tau\Delta t^2 - (18\beta + 2)\tau^2\Delta t - 6\beta\tau^3$	$(2\beta - 2\gamma + 1)\Delta t^3$
z^1	$8\beta\Delta t^3 + (18\beta + 2\gamma)\tau\Delta t^2 + (18\beta + 1)\tau^2\Delta t + 6\beta\tau^3$	0
z^0	$- 2\beta\Delta t^3 - 6\beta\tau\Delta t^2 - 6\beta\tau^2\Delta t - 2\beta\tau^3$	0

and β and γ are parameters of the Newmark integration algorithm. Derivation in detail can be referred to Chen and Ricles (2009). In this study, $\gamma = 0.5$ and $\beta = 0$ were adopted, resulting in the compensator in discrete transfer function with minimal realization as

$$C_{LAE}(z) = \frac{317.3z^2 - 608.8z + 292.6}{z^2} \quad (17)$$

where z is the complex variable in the z-domain.

4.1.2 First-order inverse compensator

Chen (2007) derived a simplified first-order discrete transfer function for servo-hydraulic systems by assuming a constant delay between the command and achieved displacements. The achieved displacement response of a servo-hydraulic actuator at the current time step can be predicted by the achieved displacement at the previous step as well as an interpolated relation between the command displacement at the current time step and the achieved displacement at the previous time step. The discrete transfer function from the command to the achieved displacements of the servo-hydraulic system can be obtained by applying the z-transform. Finally, the inverse compensator (IC) is realized by directly exchanging the polynomials in the denominator and numerator of the transfer function. As mentioned above, the nominal transfer function of the servo-hydraulic system adopted in this study has 24 delay time steps with 2,000 Hz sampling rate. Accordingly, the first-order inverse compensator can be obtained as

$$C_{IC}(z) = \frac{25z\text{-}24}{z} \quad (18)$$

4.1.3 Second-order phase-lead compensator

Similar to the first-order inverse compensator, Chen and Tsai (2013) proposed the second-order phase-lead compensator (PLC) by using weighted linear extrapolation and the inverse model principle in which the two weightings W_1 and W_2 in the derived stable region need to be selected. The PLC can be expressed as

$$C_{PLC}(z) = \frac{[W_1 + (W_1 + W_2 + 1)\alpha]z^2 + [W_2 - (W_1 + W_2 + 1)\alpha]z + 1}{W_1 z^2 + W_2 z + 1} \quad (19)$$

A delay constant α was assigned 24 for the PLC since there is 24 delay time steps in the nominal transfer function of the servo-hydraulic system. The weightings W_1 and W_2 were set 3 and 2, respectively which are located in the stable region. Accordingly, the PLC can be obtained as

$$C_{PLC}(z) = \frac{147z^2 - 142z + 1}{3z^2 + 2z + 1} \quad (20)$$

4.2 Bilinear transform

The robust stability analysis method introduced previously is applicable to continuous-time systems; however, the three delay compensation methods are based on discrete time. As a result, conversion from discrete time to continuous time for the compensators is essential to conducting the robust stability analysis. Conversion methods such as zero-order hold and first-order hold have been commonly adopted in practice. However, these two methods may not have acceptable agreement in the frequency domain between the continuous-time and discrete-time models, resulting in significant discrepancy of

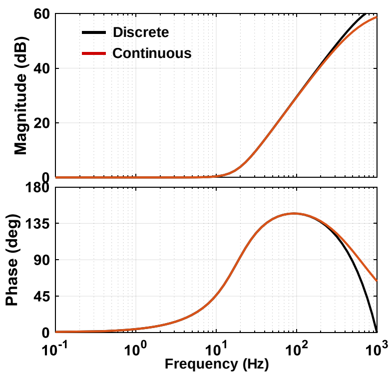

(a) Linear acceleration extrapolation

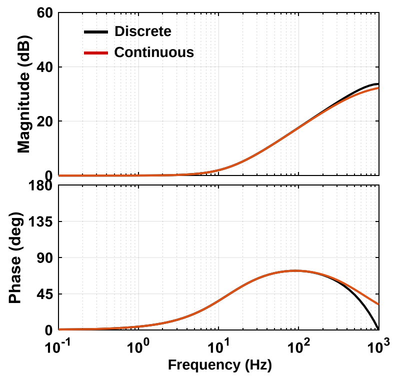

(b) Inverse compensator

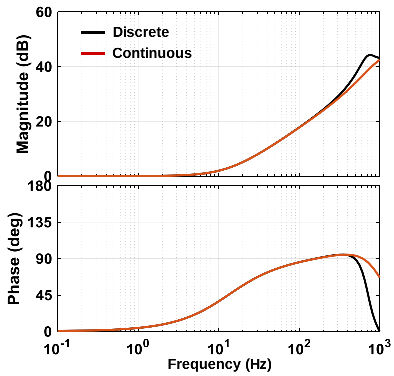

(b) Phase-lead compensator

Fig. 9 Bode diagram of the delay compensators in discrete and continuous time robust stability analysis results. In this study, bilinear transform, also called Tustin's method, was adopted to convert the discrete-time compensators to continuous-time compensators as it yields excellent match between the continuous-time and discrete-time systems in the frequency domain (Oppenheim *et al*. 1999). The bilinear transform relates the *s*-domain and *z*-domain transfer function by

$$z = e^{sT_s} = \frac{e^{\frac{sT_s}{2}}}{e^{-\frac{sT_s}{2}}} \approx \frac{1 + \frac{sT_s}{2}}{1 - \frac{sT_s}{2}} \tag{21}$$

where T_s is the sample time of the discrete-time model. Figs. 9(a)-(c) shows the Bode diagram of the three delay compensators in discrete and continuous time. It is observed that the converted continuous-time transfer function fits the discrete-time delay compensator well when the frequency is smaller than 250 Hz. As a result, the robust stability analysis is applicable and representative with a frequency range between 0 Hz to 250 Hz.

4.3 Robust stability

The robust stability margin with respect to the relationship between the natural frequency of the entire structure and the stiffness ratio p_k can be obtained by following the same procedure introduced previously. Fig. 10 shows the associated analytical results. For the nominal servo-hydraulic system, it is found that the entire stiffness of the structure can be physically tested by applying the LAE compensator with the natural frequency of the structure that ranges from 0 Hz to 20 Hz. On the other hand, the second-order PLC performs slightly better than the first-order IC. It is worth noting that the second-order PLC can be approximated to the first-order IC if a large weighting W_1 and a small weighing W_2 are adopted. The compensation performance of the PLC is changed by selecting different weightings. The effects of different weightings for the PLC have been discussed in detail by Chen *et al.* (2014). Nevertheless, the allowable stiffness ratio p_k decreases significantly when the natural frequency of the structure is larger than 8 Hz for both IC and PLC. For the system with uncertainty, 100% of the structural stiffness still can be physically tested in RTHS compensated by the three delay compensation methods when the natural frequency of the structure is smaller than 1.8 Hz. However, the allowable stiffness ratio p_k decreases significantly when the natural frequency of the structure ranges from 1.8 Hz to 10 Hz. It also shows that stable RTHS can be achieved for a stiff structure (natural frequency equals 20 Hz) with a stiffness ratio p_k larger than 10% by applying the LAE compensation method. Conclusively, delay compensation methods are helpful to increasing the allowable stiffness ratio that retains stable RTHS. However, the stable margin is significant affected by the system uncertainty especially when the natural frequency of the structure is within 2 Hz to 8 Hz. It is suggested that system uncertainty must be considered for stability analysis of RTHS if the experimental substructure merely contributes the stiffness term to the entire structure.

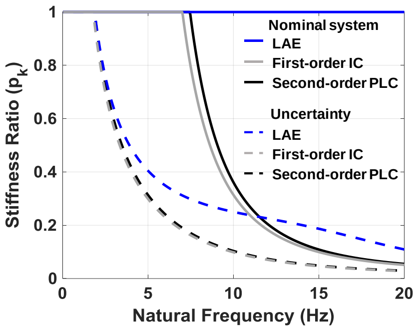

Fig. 10 Stability margin of RTHS in terms of stiffness ratio considering system uncertainty and delay compensation

5. Experimental verification

The robust stability margin of RTHS of a SDOF structure with part of the stiffness tested experimentally was further verified in the laboratory.

5.1 Experimental setup and system identification

The experimental setup for verifying the robust stability margin was identical to that adopted in the study by Chen and Tsai (2013) as shown in Fig. 11. In the setup, the dynamic servo-hydraulic actuator used to drive the shake table has maximum stroke and force capacity of ±127 mm and ±15 kN, respectively. An MTS FlexTest Controller FT-100 digital controller was used to control the actuator by well-tuned proportional, integral, and derivative gains. A steel plate with a dimension of 630 mm × 250 mm ×10 mm was installed on the shake table to represent the experimental substructure with the stiffness term in RTHS. A dSPACE DS1103, which is a real-time computation system, was used to perform the RTHS as it is well-supported by Real-Time Interface for MATLAB/Simulink. In this experimental verification, the numerical substructure and the delay compensation were implemented by Simulink models with real-time input/output blocks. The sampling frequency and solver adopted in the RTHS were 2,000 Hz and the ode5 solver, respectively.

System identification test was first conducted to identify the dynamics of servo-hydraulic system. The input command displacement was a band-limited white noise with a frequency range from 0 to 30 Hz and a root-mean-

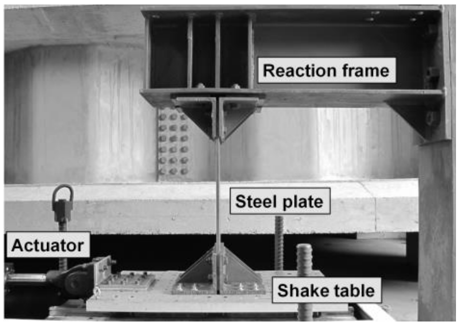

Fig. 11 Experimental setup for the verification

square power of 0.15 mm. During the system identification test, the data were collected with a sampling rate of 1,024 Hz in 600 seconds. While processing data, 16,384 FFT points, a Hanning window with 50% overlap, and 74 averages were used in system identification. Consequently, a four-pole transfer function was identified as

$$G_s(s) = \frac{1.942 \cdot 10^{10}}{s^4 + 954.5s^3 + 5.712 \cdot 10^5 s^2 + 1.716 \cdot 10^8 s + 1.942 \cdot 10^{10}} \tag{22}$$

Fig. 12 depicts the identification result which demonstrates reasonable agreement with the testing result. It can be evaluated that the nominal transfer function had an approximate constant delay of 18 time steps with 2,000 Hz sampling rate in RTHS. Accordingly, the transfer function in Eq. (22) was adopted as the nominal servo-hydraulic system for conducting robust stability analysis and designing the three aforementioned delay compensators. Similar to the numerical simulation in the previous section, the perturbed nominal transfer function of the servo-hydraulic system was obtained by assuming ±10% identification error as the parametric uncertainty for each parameter in Eq. (22). The damping ratio of the SDOF structure in RTHS was assumed 2%. Finally, the stability margin of the experimental example can be realized by following the proposed robust stability analysis procedure. The resulted robust stability margin of RTHS in terms of stiffness ratio considering system uncertainty and delay compensation is shown in Fig. 13.

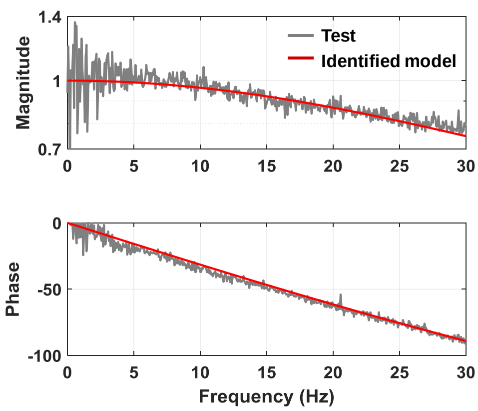

Fig. 12 Frequency response of the identified model

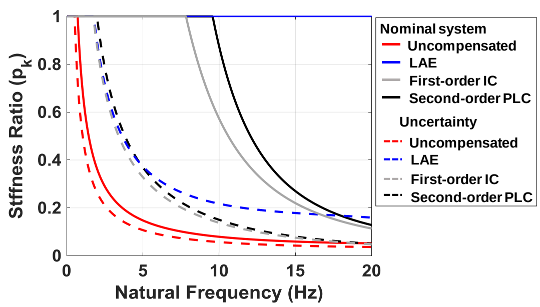

Fig. 13 Stability margin of RTHS in the experimental verification

5.2 Experimental results

In order to demonstrate that the stability margin obtained without considering system uncertainty is not conservative enough for conducting RTHS, various RTHS tests were conducted. First, the natural frequency of the SDOF structure (ω_n) was set 5 Hz. From Fig. 13, it can be found that the corresponding allowable stiffness ratios with and without considering system uncertainty (p_{ku} and p_{kn}) are 0.11 and 0.15, respectively. Accordingly, three stiffness ratios (p_k) in the verifying RTHS were selected including 0.08, 0.14, and 0.20. Noted that the stiffness ratio of 0.08 is smaller than the robust allowable stiffness ratio; 0.14 is between the robust and nominal allowable stiffness ratios; and 0.20 is larger than the nominal allowable stiffness ratio. In the verifying RTHS, the El Centro earthquake record with a normalized peak ground acceleration of 1m/s^2 was used to excite the SDOF structure. Fig. 14 shows the experimental results. It is found that when the stiffness ratio (0.08) is smaller than the robust allowable stiffness ratio (0.11), the RTHS result is stable. Meanwhile, when the stiffness ratio (0.14) is between the robust and nominal allowable stiffness ratios (0.11 and 0.15), it is not stable in this verifying example. The result demonstrates that the allowable stiffness ratio obtained from the nominal transfer function of servo-hydraulic system does not definitely guarantee the stability of RTHS. Lastly, when the stiffness ratio (0.20) is larger than the nominal allowable stiffness ratio (0.15), the RTHS is unstable. However, the RTHS became stable when the three delay compensation methods were applied as shown in Fig. 15. The stable results can be also confirmed by checking the stability margin in Fig. 13 in which the stiffness ratio of 0.20 is smaller than the three robust allowable stiffness ratios after applying the three compensation methods. Then, the natural frequency of the SDOF structure (ω_n) was changed to 15 Hz and the stiffness ratio was retained 0.20. In this case, the stiffness ratio is between the robust and nominal allowable stiffness ratios after applying the three compensation methods as indicated in Fig. 13. The corresponding RTHS results are shown in Fig. 16 which demonstrates the entire RTHS loop is unstable for each delay compensation case. It demonstrates again that the allowable stiffness ratio without considering system uncertainty does not absolutely assure the stability

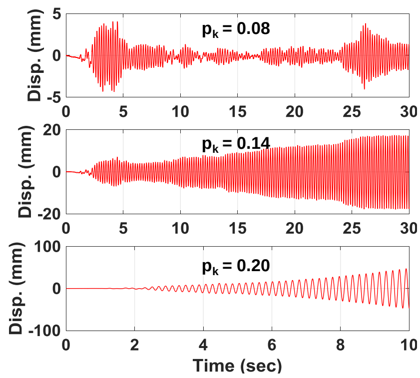

Fig. 14 Uncompensated RTHS results with different stiffness ratios (ω_n = 5 Hz)

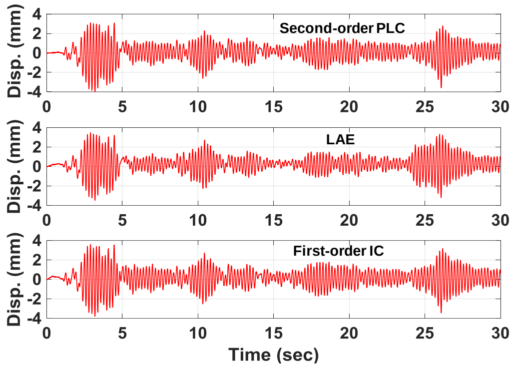

Fig. 15 Compensated RTHS results
(p_k = 0.20 and ω_n = 5 Hz)

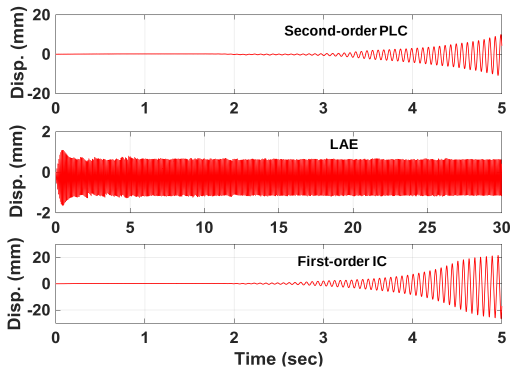

Fig. 16 Compensated RTHS results
(p_k = 0.20 and ω_n = 15 Hz)

of RTHS. Conclusively, the proposed robust stability analysis method provides a strong and conservative stability margin for RTHS which has been verified experimentally.

6. Robust stability analysis (mass and damping terms)

6.1 Specimen in mass term

Consider a SDOF structure in which part of the mass is experimentally tested. Hence, the equation of motion of the SDOF structure can be expressed as

$$\begin{aligned}&(1-p_m)m\ddot{x}(t)+c\dot{x}(t)+kx(t)\\&=-m\ddot{x}_g(t)-p_m m\ddot{x}(t)\end{aligned} \quad (23)$$

where p_m is the ratio of the mass of the experimental substructure to the entire mass of the SDOF structure. Also, p_m is called the mass ratio in the study for simplicity purposes. Accordingly, the transfer function of the numerical substructure in Fig. 4 becomes

$$G_{ns}(s)=\frac{-1}{(1-p_m)s^2+2\xi\omega_n s+\omega_n^2} \quad (24)$$

By applying the procedure of robust stability analysis with identical parametric uncertainty and weight function $W(s)$, the robust stability margin in terms of the mass ratio can be obtained as shown in Fig. 17. For the nominal servo-hydraulic system, it is found that merely less than 75% of mass can be physically tested and the allowable mass ratio decreases when the natural frequency of the structure increases. However, the variation of allowable mass ratio with respect to the natural frequency is not as sensitive as the stiffness ratio is. More than 63% of mass can still be experimentally tested in RTHS when the natural frequency of the structure is 20 Hz. For the servo-hydraulic system with uncertainty, merely the inferior allowable mass ratio is discussed and adopted for the following analyses with delay compensation in RTHS. It can be found that the allowable mass ratio considering system uncertainty is smaller than that of the nominal system. However, more than 46% of the entire structural mass can be tested as an experimental substructure in RTHS. Similarly, the robust stability margin in terms of the mass ratio with delay compensation can be obtained by following the same procedure. Fig. 18 shows the stability margin of RTHS in terms of mass ratio considering system uncertainty and delay compensation. For the nominal system without uncertainty, it shows that the allowable mass ratio with delay compensation becomes smaller than that without delay compensation. The allowable mass ratio of the RTHS compensated by LAE is almost identical to that without compensation from 0 Hz to 8 Hz; however, it starts to drop significantly when the natural frequency is larger than 8 Hz. Meanwhile, the allowable mass ratio of the IC and PLC cases are frequently inferior to the case without compensation except that the has slightly larger allowable mass ratio when the

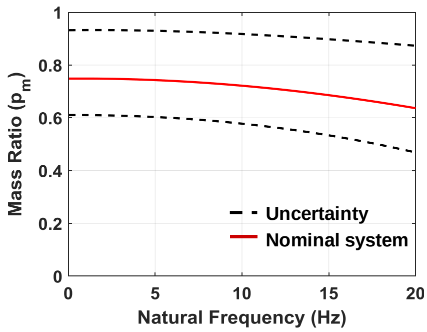

Fig. 17 Stability margin of RTHS in terms of mass ratio considering system uncertainty

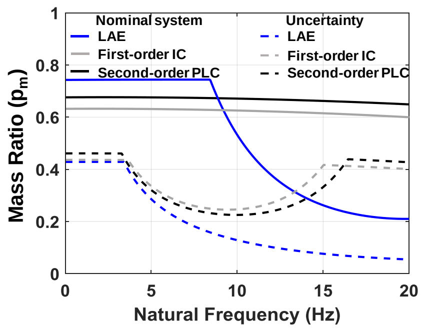

Fig. 18 Stability margin of RTHS in terms of mass ratio considering system uncertainty and delay compensation

natural frequency is larger than 18 Hz. For the system considering uncertainty, all the three delay compensators have smaller allowable mass ratio than the uncompensated RTHS. Surprisingly, both the allowable mass ratio of IC and PLC decrease from 3.2 Hz to almost 10 Hz and then start to increase at 10 Hz. This phenomenon is not observed in the LAE case. Summarily, it indicates that the mass ratio which can be experimentally tested in a stable RTHS becomes even small when the delay compensator is applied. As a result, delay compensation may not be necessary for RTHS with part of the mass tested experimentally.

6.2 Specimen in damping term

Similarly, consider a SDOF structure in which part of the damping is experimentally tested. Therefore, the equation of motion of the SDOF structure can be represented as

$$\begin{aligned} & m\ddot{x}(t) + (1 - p_c)c\dot{x}(t) + kx(t) \\ & = -m\ddot{x}_g(t) - p_c c\dot{x}(t) \end{aligned} \tag{25}$$

where p_c is the ratio of the damping coefficient of the experimental substructure to the entire damping coefficient of the SDOF structure. Likewise, p_c is named the damping coefficient ratio in the study. Consequently, the transfer function of the numerical substructure in Fig. 4 becomes

$$G_{ns}(s) = \frac{-1}{s^2 + 2\xi\omega_n(1 - p_c)s + \omega_n^2} \tag{26}$$

Again, the robust stability margin in terms of the damping coefficient ratio can be obtained by applying the same procedure of robust stability as shown in Fig. 19. For the nominal servo-hydraulic system, it is found that 100% of damping can be physically tested without unstable issue for RTHS even though the inherent damping ratio of the SDOF structure was assumed merely 2%. However, when the system uncertainty is considered, the allowable damping coefficient ratio starts to decrease when the natural frequency of the structure is larger than 16 Hz. More than 76% of damping can still be experimentally tested in RTHS when the natural frequency of the structure is 20 Hz. It can be concluded that a stable RTHS is not difficult to achieve when the physical specimen merely contributes damping force to the entire structure such as magnetorheological dampers. However, a stable RTHS is not necessarily equivalent to a successful RTHS as the dynamics of the servo-hydraulic system could distort the RTHS results seriously due to tracking error. When the three delay compensation methods were further considered, the analysis results indicated that all the RTHS cases were robustly stable with 100% damping tested experimentally and a natural frequency of structure ranged from 0 Hz to 20 Hz.

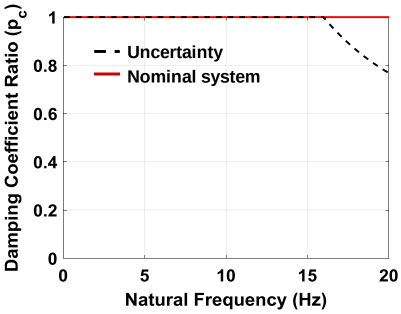

Fig. 19 Stability margin of RTHS in terms of damping coefficient ratio considering system uncertainty

7. Conclusions

Real-time hybrid simulation (RTHS) has been attracting the attention of researchers in earthquake engineering and become an alternative experimental method to investigate seismic responses of structures subjected to dynamic loadings. RTHS forms a closed loop in which the servo-hydraulic system, numerical substructure, and experimental substructure are involved. The time delay or lag of the servo-hydraulic system introduce negative damping into the closed loop and result in potential instabilities of a RTHS. Although various methods have been proposed for evaluating the stability of a RTHS, they are mostly based on known and persistent dynamics of the servo-hydraulic system which is generally obtained by conducting system identification. However, uncertainty of a servo-hydraulic system exists inevitably in real practice which could misrepresent the evaluation of stability in a RTHS. In this paper, a robust stability analysis procedure is proposed to evaluate the stability margin of a RTHS considering the uncertainty of the servo-hydraulic system. Parametric uncertainty is adopted to parametrize the coefficients of the servo-hydraulic system transfer function within a predefined range which varies from test to test and can be determined by users. The variation of servo-hydraulic system dynamics is then bounded by a multiplicative uncertainty model which contains a predefined stable weight function and a random stable transfer function considering magnitude and phase perturbation. A simple and effective method for selecting the weight function without trial and error is proposed in this study. Afterwards, the Nyquist plot with multiplicative uncertainty is utilized to realize the stability of RTHS with system uncertainty. Finally, three common delay compensation methods are adopted in the RTHS stability analysis. The robust stability margin is interpreted as an allowable ratio of stiffness, mass, and damping coefficient of the experimental substructure to the entire structure.

The analytical results demonstrate that the allowable stiffness ratio decreases significantly when the natural frequency of the structure increases from 0.5 Hz to 5 Hz which represents the first natural frequency of civil structures in real practice. It indicates that delay compensation is indispensable for completing a stable RTHS if the physical specimen merely contributes the stiffness term. The allowable stiffness ratio becomes even restricted if the system uncertainty is considered. Meanwhile, the allowable stiffness ratio can be increased effectively by applying the three compensation methods. The physical specimen can contribute 100% stiffness of the structure without meeting stability problems as far as the natural frequency of the structure is smaller than 7 Hz. In addition, RTHS with LAE compensator is permanently stable within the natural frequency of the structure from 0 Hz to 20 Hz. However, the allowable stiffness ratio of RTHS begins to decrease significantly when the natural frequency of the structure is larger than 1.8 Hz if the system uncertainty is considered. It demonstrates that the physical specimen in a RTHS considering system uncertainty is not able to represent 100% stiffness of the entire structure with a natural frequency larger than 1.8 Hz even delay compensation is applied. Nonetheless, the analyses also designate that delay compensation is helpful to improving the stability margin of RTHS under system uncertainty. The proposed robust stability margin was also verified by conducting RTHS in the laboratory. Experimental results indicated that the allowable stiffness ratio without considering system uncertainty does not absolutely assure the stability of RTHS while the allowable stiffness ratio considering system uncertainty provides an assertive stability margin for RTHS. On the other hand, the allowable mass ratio does not vary significantly with different natural frequencies of structures. More than 63% of mass can be experimentally tested in RTHS within the natural frequency of the structure from 0 Hz to 20 Hz. In addition, more than 46% of the entire structural mass can still be tested within the natural frequency of the structure from 0 Hz to 20 Hz even the system uncertainty is considered in the stability analysis. Furthermore, the allowable mass ratio becomes even smaller when the three delay compensators are applied which shows that delay compensation is not effective for RTHS with part of the mass tested experimentally. Lastly, analytical results demonstrate that 100 % of damping can be experimentally tested in RTHS within the natural frequency of the structure from 0 Hz to 20 Hz with or without delay compensation. When the system uncertainty is considered, more than 76% of damping can still be experimentally tested in RTHS without delay compensation when the natural frequency of the structure is 20 Hz. It indicates that a stable RTHS can be achieved effortlessly if the experimental specimen merely contributes the damping force to the entire structure. Summarily, a modeling and robust stability analysis method for RTHS has been proposed and used to evaluate the stability margin in terms of the allowable stiffness, mass, and damping coefficient ratios. The study provides the practitioners who would like to apply RTHS for experimental studies with a simple and straightforward approach to identify the robust stability margin before the RTHS is conducted.

Acknowledgments

The authors would like to thank the funding supported by the Ministry of Science and Technology, Republic of China (Taiwan) (MOST 106-2221-E-011 -165 -MY2).

References

Carrion, J.E. and Spencer, B.F. (2007), “Model-based strategies for real-time hybrid testing”, No. 6; Newmark Structural Engineering Laboratory Report Series, University of Illinois at Urbana-Champaign, Urbana, IL, USA.

Chae, Y., Kazemibidokhti, K. and Ricles, J.M. (2013), “Adaptive time series compensator for delay compensation of servo-hydraulic actuator systems for real-time hybrid simulation”, *Earthq. Eng. Struct. Dyn.*, **42**(11), 1697-1715. https://doi.org/10.1002/eqe.2294

Chen, C. (2007), “Development and numerical simulation of hybrid effective testing method.”, Ph.D. Dissertation; Lehigh University, Bethlehem, PA, USA.

Chen, C. and Ricles, J.M. (2008), “Stability analysis of SDOF real-time hybrid testing systems with explicit integration algorithms and actuator delay”, *Earthq. Eng. Struct. Dyn.*, **37**(4), 597-613. https://doi.org/10.1002/eqe.775

Chen, C. and Ricles, J.M. (2009), “Analysis of actuator delay compensation methods for real-time testing”, *Eng. Struct.*, **31**(11), 2643-2655. https://doi.org/10.1016/j.engstruct.2009.06.012

Chen, P.C. and Tsai, K.C. (2013), “Dual compensation strategy for real-time hybrid testing”, *Earthq. Eng. Struct. Dyn.*, **42**(1), 1-23. https://doi.org/10.1002/eqe.2189

Chen, C., Ricles, J.M., Marullo, T.M. and Mercan, O. (2009), “Real-time hybrid testing using the unconditionally stable explicit CR integration algorithm.”, *Earthq. Eng. Struct. Dyn.*, **38**(1), 23-44. https://doi.org/10.1002/eqe.838

Chen, P.C., Tsai, K.C. and Lin, P.Y. (2014), “Real-time hybrid testing of a smart base isolation system”, *Earthq. Eng. Struct. Dyn.*, **43**(1), 139-158. https://doi.org/10.1002/eqe.2341

Doyle, J., Francis, B. and Tannenbaum, A. (1992), *Feedback Control Theory*, Macmillan, New York, NY, USA.

Gonzalez-Buelga, A., Wagg, D.J. and Neild, S.A. (2007), “Parametric variation of a coupled pendulum–oscillator system using real-time dynamic substructuring”, *Struct. Control Health Monitor.*, **14**(7), 991-1012. https://doi.org/10.1002/stc.189

Hayati, S. and Song, W. (2017), “An optimal discrete-time feedforward compensator for real-time hybrid simulation”, *Smart Struct. Syst., Int. J.*, **20**(4), 483-498. https://doi.org/10.12989/sss.2017.20.4.483

Horiuchi, T. and Konno, T. (2001), “A new method for compensating actuator delay in real-time hybrid experiments”, *Philosophical Transactions of the Royal Society of London, Series A: Mathematical, Physical and Engineering Sciences*, **359**, 1786-1893. https://doi.org/10.1098/rsta.2001.0878

Horiuchi, T., Inoue, M., Konno, T. and Namita, Y. (1999), “Real-time hybrid experimental system with actuator delay compensation and its application to a piping system with energy absorber”, *Earthq. Eng. Struct. Dyn.*, **28**(10), 1121-1141. https://doi.org/10.1002/(SICI)1096-9845(199910)28:10<1121::AID-EQE858>3.0.CO;2-O

Huang, L., Chen, C., Guo, T. and Chen, M. (2019), “Stability analysis of real-time hybrid simulation for time-varying actuator delay using the Lyapunov-Krasovskii functional approach”, *J. Eng. Mech.*, **145**(1), 04018124. https://doi.org/10.1061/(ASCE)EM.1943-7889.0001550

Jung, R.Y., Shing, P.B., Stauffer, E. and Bradford, T. (2007), “Performance of a real-time pseudodynamic test system considering nonlinear structural response”, *Earthq. Eng. Struct. Dyn.*, **36**(12), 1785-1809. https://doi.org/10.1002/eqe.722

Maghareh, A., Dyke, S.J., Rabieniaharatbar, S. and Prakash, A. (2017), “Predictive stability indicator: a novel approach to configuring a real-time hybrid simulation”, *Earthq. Eng. Struct. Dyn.*, **46**(1), 95-116. https://doi.org/10.1002/eqe.2775

Mercan, O. and Ricles, J.M. (2007), “Stability and accuracy analysis of outer loop dynamics in real-time pseudodynamic testing of SDOF systems”, *Earthq. Eng. Struct. Dyn.*, **36**(11), 1523-1543. https://doi.org/10.1002/eqe.701

Merritt, H.E. (1967), *Hydraulic Control Systems*, Wiley, New York, USA.

Oppenheim, A.V., Schafer, R.W. and Buck, J.R. (1999), *Discrete-*

Time Signal Processing, Prentice Hall, NJ, USA.

Phillips, B.M., Takada, S., Spencer, B.F. and Yozo, F. (2014), "Feedforward actuator controller development using the backward-difference method for real-time hybrid simulation", *Smart Struct. Syst., Int. J.*, **14**(6), 1081-1103. https://doi.org/10.12989/sss.2014.14.6.1081

Rekasius, Z.V. (1980), "A stability test for systems with delay", *Proceedings, Joint Automatic Control Conference*, San Francisco, CA, USA, Paper no. TP9-A.

Tang, Z., Dietz, M. and Li, Z. (2018), "Substructuring stability analysis in light of comprehensive transfer system dynamics", *Bull. Earthq. Eng.*, **16**(1), 129-154. https://doi.org/10.1007/s10518-017-0192-9

Wallace, M.I., Sieber, J., Nield, S.A., Wagg, D.J. and Krauskopf, B. (2005), "Stability analysis of real-time dynamic substructuring using delay differential equations", *Earthq. Eng. Struct. Dyn.*, **34**(15), 1817-1832. https://doi.org/10.1002/eqe.513

Zhou, K. and Doyle, J. (1998), *Essentials of Robust Control*, Prentice Hall, New Jersey, USA.

Zhu, F., Wang, J.T., Jin, F., Chi, F.D. and Gui, Y. (2015), "Stability analysis of MDOF real-time dynamic hybrid testing systems using the discrete-time root locus technique", *Earthq. Eng. Struct. Dyn.*, **44**(2), 221-241. https://doi.org/10.1002/eqe.2467

BS